

Ultrafast Vibrational Spectroscopy of Cyanophenols

Kyung-Koo Lee,[†] Kwang-Hee Park,[†] Jun-Ho Choi,[†] Jeong-Hyon Ha,[‡] Seung-Joon Jeon,^{†,‡} and Minhaeng Cho^{*,†,‡}

Department of Chemistry, Korea University, Seoul 136-701, Korea, and Multidimensional Spectroscopy Laboratory, Korea Basic Science Institute, Seoul 136-713, Korea

Received: September 8, 2009; Revised Manuscript Received: January 17, 2010

Aromatic compounds with electron-donating or -accepting substituents exhibit interesting resonance effects on a variety of chemical reactivities and optical properties. To understand such effects and the possible relationship between vibrational energy dissipation pathways and resonance structures of aromatic compounds, we studied ortho-, meta-, and para-substituted cyanophenols and their anionic forms in methanol by using time- and frequency-resolved pump–probe and two-dimensional IR spectroscopy, where the nitrile group acts as an IR probe. From the measured transient spectra and singular-value decomposition analyses, we found that there is a combination band whose frequency is very close to that of the nitrile stretch mode. Due to the difference in the lifetimes of these two mode excited states, the transient pump–probe spectra commonly show notable blue-shifting behaviors in time. Comparing the vibrational lifetimes of neutral cyanophenols and cyanophenoxyde anions in methanol and carrying out quantum mechanical/molecular mechanical molecular dynamics simulations to study hydrogen-bonding dynamics, we found that the vibrational energy of the nitrile stretch mode initially relaxes to intramolecular degrees of freedom instead of solvent modes. Also, the vibrational anharmonic frequency shifts, intrinsic lifetimes, and bandwidths of the nitrile stretch mode and the combination mode in these molecular systems are fully characterized, and their relationships with resonance structures are discussed. It is believed that the present work sheds light on the intrinsic vibrational relaxation process of the nitrile stretch mode in cyanophenols, even in the case when their IR spectra are congested by the spectrally overlapping combination bands, and the resonance effects of aromatic compounds on vibrational dynamics and relaxation processes.

Introduction

Aromatic substitution reactions, various nonlinear optical properties of donor–acceptor conjugated polyenes, and organic light-emitting diodes are a few examples showing the importance of resonance structures of aromatic or conjugate polyene molecules.^{1–10} In particular, the chemical reactivity of aromatic compound is strongly affected by the substituted electron-donating or -accepting groups.^{11–14} Such chemical reactions involve a number of intra- and intermolecular processes, but one of the early events in a given chemical reaction is the dissipation of excess energy of the transition state to other intramolecular modes or to bath modes that are anharmonically coupled to the initially excited vibrational modes. Thus, in addition to the intramolecular vibrational relaxation, it is critical to understand how the energy accumulated in a reactive species dissipates into bath degrees of freedom and particularly how such processes are related to the resonance structure formation and induction effects.

To understand the energy relaxation channels in disubstituted aromatic compounds in solutions, we chose cyanophenols, where nitrile and hydroxyl groups are the two substituents (see Figure 1). Here, the *n*-cyanophenol and *n*-cyanophenoxyde anions will be denoted as *n*CP and *n*CX, respectively. Among them, we recently studied nitrile stretching vibrations of 4CP and 4CX in methanol solutions by using the integrated and dispersed

photon echo methods and determined vibrational lifetimes and overtone anharmonicities of the CN stretch modes in these compounds.¹⁵ However, it is not possible to study the heterogeneous nature of vibrational states when there are spectrally overlapping IR-active modes, and in such a case, one cannot obtain the corresponding eigenspectra.

In cyanophenols, the nitrile group acts as an electron-accepting group, whereas the hydroxyl group is a weak electron donor in these cases. If a given cyanophenol becomes an anion in solution at a high pH, the phenoxy oxygen atom becomes a strong electron-donating group so that 2CX and 4CX are stabilized by the resonance structures,¹⁶ as shown in Figure 1. In this paper, we shall present experimental results on these six different compounds dissolved in methanol, where we used transient infrared pump–probe spectroscopic techniques and focused on the nitrile stretch vibrations. To obtain the time-resolved spectra, the pump–probe signal field was first dispersed, and then its spectrum was recorded with an array detector. The nitrile stretch vibration has attracted a great deal of attention recently because it can be an ideal IR probe for studying conformational transitions of proteins,^{17–21} enzyme–inhibitor binding to HIV-1 reverse transcriptase,²² and structure determination of nitrile-substituted DNA oligomers.²³ Furthermore, the hydrogen-bond forming and breaking in a acetonitrile/methanol solution has been studied by using a two-dimensional IR spectroscopic method.^{24–26}

Although we have also measured the 2D IR spectra of a few selected molecules in Figure 1, we found that the frequency-resolved pump–probe spectroscopy is enough to study the nitrile stretching vibrations in the cyanophenols. A typical transient

* To whom correspondence should be addressed. E-mail: mcho@korea.ac.kr. Fax: +82-2-3290-3121.

[†] Korea University.

[‡] Korea Basic Science Institute.

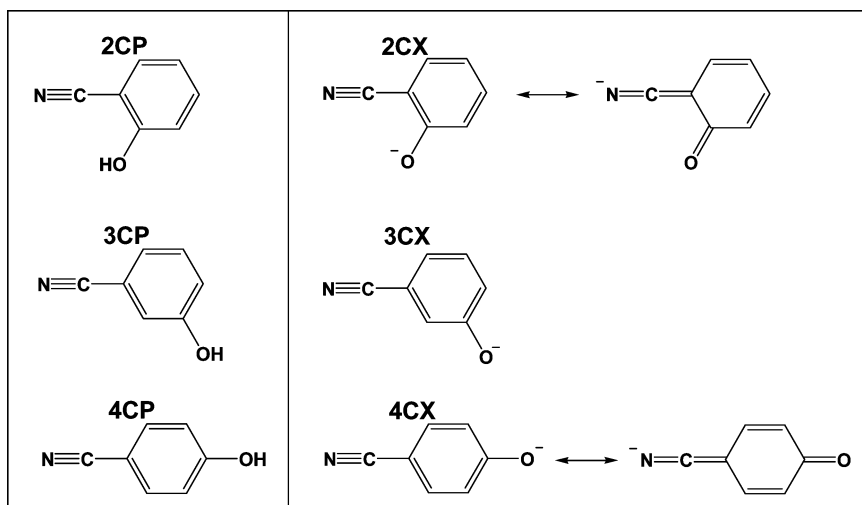


Figure 1. Molecular structures of *n*-cyanophenols. On the right-hand side of this figure, their anionic forms are shown with corresponding resonance structures.

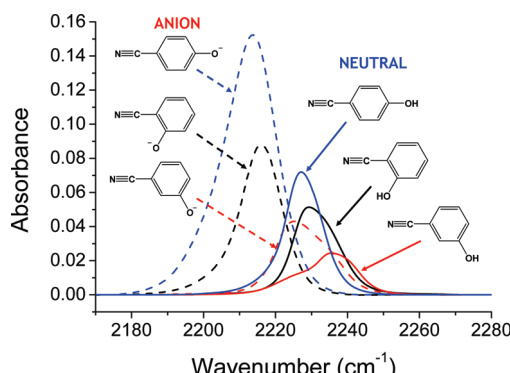


Figure 2. IR absorption spectra of the nitrile stretch mode. The solution concentration is 0.1 M. Dashed lines are those of *n*-cyanophenoxydes in methanol, whereas the solid lines are those of neutral cyanophenols.

pump–probe (PP) spectrum of an anharmonic oscillator shows both positive and negative peaks that are associated with 0–1 and 1–2 transitions, respectively.^{27,28} Here, the ground, first excited, and second excited (overtone) states are denoted as $|0\rangle$, $|1\rangle$, and $|2\rangle$, respectively. The positive peak originates from both ground-state bleach and stimulated emission contributions, whereas the negative peak is from excited-state absorption. The frequency difference between the positive and negative peaks is related to both an overtone anharmonic frequency shift and the spectral bandwidth.²⁷ In this work, we will present experimentally measured PP spectra of six compounds (2CP–4CX) in methanol with respect to the delay time T from 0 up to tens of picoseconds. Interestingly, depending on the relative position of the substituent OH group with respect to the CN group, the vibrational dynamics of the C–N stretch mode changes. Furthermore, upon ionization of these cyanophenols at high pH, their lifetimes and transient PP spectral line shapes show notable features that can be related to the resonance effects mentioned above.

Experimental Results

Infrared Absorption. In Figure 2, the CN stretch IR bands (solid lines) of neutral cyanophenols in methanol solutions are presented. Here, the solution concentration is 0.1 M. The peak frequencies of 2CP, 3CP, and 4CP are 2230, 2236, and 2227 cm^{-1} , respectively. The dashed lines in this figure are the IR

bands of their anionic forms, 2CX, 3CX, and 4CX, and their peak frequencies are 2216, 2225, and 2214 cm^{-1} . The cyanophenoxydes were prepared by adding excessive sodium methoxide to the solutions. The peak frequencies already show an interesting dependency of the nitrile stretch frequency on the molecular structure. When the OH group in CP or the O[−] anion in CX is substituted at the para position with respect to the CN group, due to the resonance effects, the CN bond strength becomes diminished so that the CN stretch frequency is red-shifted. On the other hand, the meta-substituted OH or O[−] group cannot be strongly stabilized by the resonance structure formation. Thus, the magnitude of resonance effect on the CN frequency is in the following order, para > ortho > meta or 4CP > 2CP > 3CP and 4CX > 2CX > 3CX.

Second, the CN stretch frequency is strongly red-shifted when the cyanophenol becomes an anion in a high-pH solution. The frequency difference between 2CP and 2CX is 14 cm^{-1} , and those between 3CP and 3CX and between 4CP and 4CX are 11 and 13 cm^{-1} , respectively. Furthermore, all of the line shapes of the CN stretch bands appear to be asymmetric, and this indicates a heterogeneity in solvation structures, such as those with and without hydrogen bonds with methanol, or a possible existence of other vibrational states in addition to the CN stretch band. Furthermore, as will be shown below, the time-resolved PP spectra reveal that there exist two different excited states in the frequency region around the CN stretch mode for all six cases. A detailed interpretation and the underlying origin of the asymmetric line shapes of IR absorption spectra at the CN stretch band will be presented below.

Aggregate Formation. Transient IR pump–probe experiments were performed for solutions with concentration of about 0.2 M. This is a highly concentrated solution sample; therefore, it is necessary to examine the possibility of aggregate formation of these compounds in methanol solutions. We thus measured the UV–vis absorption spectra of 4CP/methanol solutions in the concentration range from 0.0001 to 0.5 M as well as the IR absorption spectra of the CN stretch mode of 4CP and 4CX for varying concentrations from 0.005 to 0.2 M (see Supporting Information). For the IR absorption measurements, the sample cell used and the path length were CaF₂ and 25 μm , respectively. Neutral and anionic cyanophenol solutions were prepared by dissolving the CPs in pure methanol and a 0.5 M methoxide solution, respectively. For the UV–visible absorption measurement, the typical detector of the UV–vis spectrometer used for

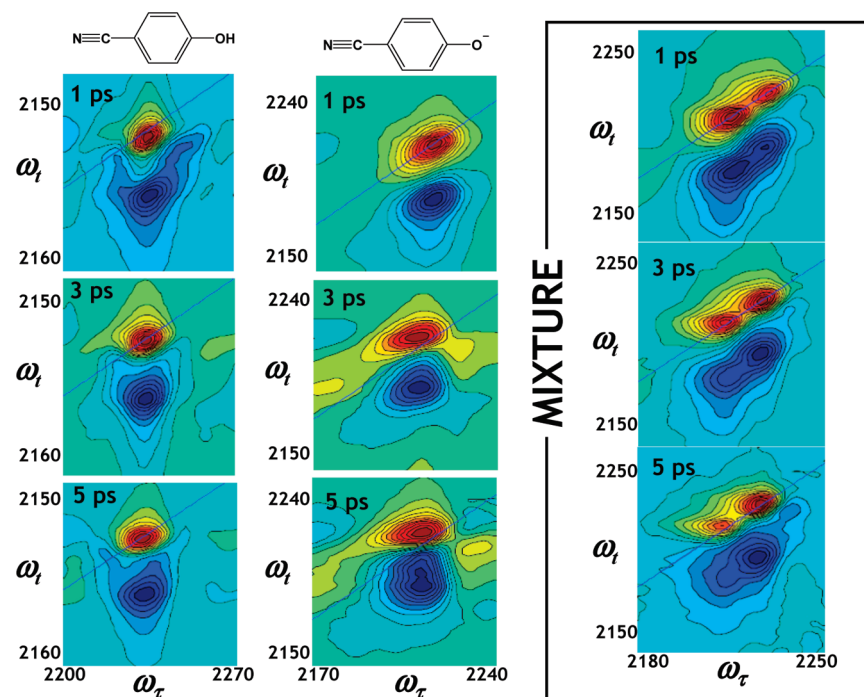


Figure 3. Two-dimensional IR spectra of 4CP (first column), 4CX (second column), and a mixture of 4CP and 4CX (third column) in methanol. The waiting time T varies from 1 to 5 ps.

the present experiment was not saturated up to the 0.1 M solution sample, but absorbance of a 0.5 M solution sample was too large to be detected. We therefore used both 1 mm and 6 μ m path length cells for such measurements. From the normalized UV-vis absorption spectra and the IR absorption spectra for varying concentrations, we found no dependency of the spectra on solute concentration, and furthermore, the integrated intensity was linearly proportional to the concentration. Second, we measured the proton NMR spectra of 4CP in methanol with varying concentrations from 5 μ M to 0.5 M. Again, there was no notable concentration dependency of the NMR spectra. These experimental results suggest that the cyanophenol molecules form neither a dimer nor an aggregate in the concentration range of interest.

Two-Dimensional IR Spectroscopy of Nitrile Stretch Mode. For the six solution samples with concentrations of \sim 0.2 M, we carried out both 2D IR and transient pump-probe experiments, where, in the latter case, the probe beam is frequency-resolved to obtain the transient PP spectra. In order to carry out these experiments, we used the same experimental setup as that used to measure the integrated and dispersed photon echo signals of 4CP in methanol.¹⁵ For both 4CP (low pH) and 4CX (high pH) solutions, we first measured a series of 2D IR spectra (see Figure 3). As usual, the positive diagonal peak representing the 0–1 transition and the negative peak representing the 1–2 transition were observed, and they appear to be diagonally elongated at a short time, which indicates short-time inhomogeneity of solvation structures.^{27,29}

Next, we carried out the same 2D IR experiments for a 4CP + 4CX mixture solution, and the series of 2D IR spectra were recorded. To prepare the solution containing both 4CP and 4CX species, we used 1 M TEA (triethylamine) and 0.5 M sodium methoxide solutions and properly added these solutions to the 4CP/methanol solution to eventually control the relative IR absorption peaks of the 4CP and 4CX to be approximately equal in magnitude. This is enough for the 2D IR experiment of the solution with 4CP and 4CX in equilibrium. Due to the frequency

difference between the CN stretch modes of 4CP and 4CX (see the blue solid and dashed lines in Figure 2), the FT-IR CN stretch band of this mixture solution is a doublet. The forward and backward reactions are the deprotonation of 4CP and protonation of 4CX. If the acid–base reaction of the phenolic OH group is fast in comparison to the vibrational population relaxation time of the CN stretch mode, which is, in the present case, the IR probe monitoring the reaction kinetics, one can directly follow this acid–base reaction by carrying out the chemical exchange 2D IR experiments.^{27,30–35}



In Figure 3 (right panel), the three snapshot 2D IR spectra of the mixture at $T = 1, 3$, and 5 ps are depicted. Here, we could find no notable cross peaks between the two CN bands of neutral and anionic cyanophenols. This indicates that the acid–base reaction in this case of the para-substituted cyanophenol in methanol is much slower than the lifetime of the CN stretch mode, \sim 2 ps. Thus, despite that we could not precisely measure the acid–base reaction rate constants in this case, they should be at least longer than a few picoseconds.

Frequency-Resolved Pump–Probe Spectroscopy. Since the broad-band PP measurements are comparatively easy and free from technical difficulties of phase-controlled four-pulse 2D IR spectroscopy, we modified the experimental setup to measure the transient frequency-resolved PP spectra for varying pump–probe delay times T from 0 to 32 ps. The contour plots of the experimentally measured PP spectra, $S(\omega, T)$, are shown in Figure 4.

Here, the x -axis represents the frequency of the dispersed pump–probe signal field, and the y -axis is the delay time T on a logarithmic scale. Since the polarization direction of the probe beam is controlled to be the so-called magic angle (54.7°) with respect to that of the pump beam, the measured PP signal decay

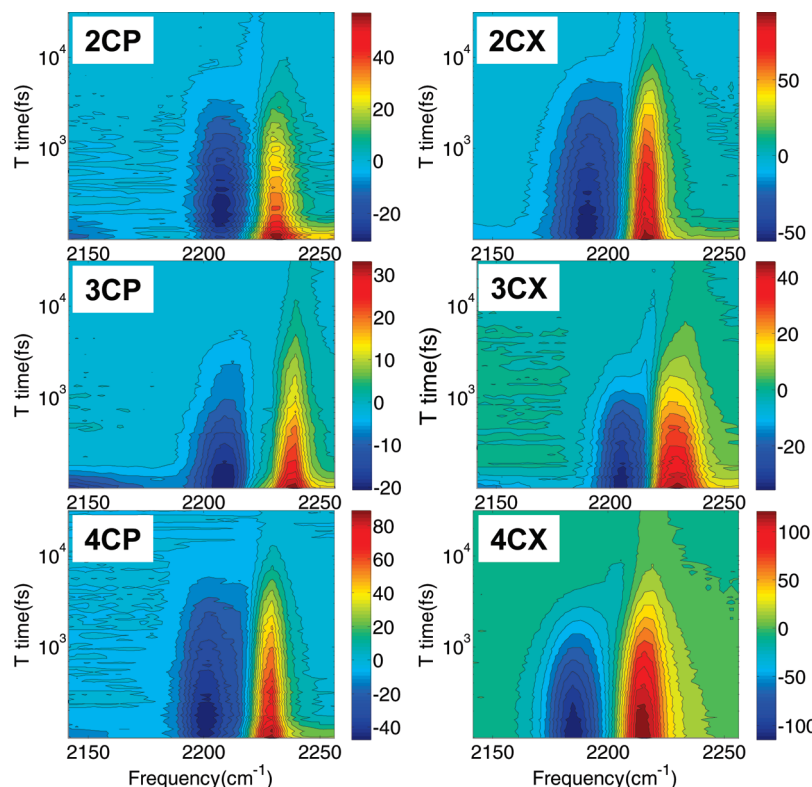


Figure 4. Time-dependent frequency-resolved pump–probe spectra. The *x*-axis is frequency in cm^{-1} , and the *y*-axis corresponds to the pump–probe delay time T in fs (on a log scale). The sample cell used and the path length are CaF_2 and $25 \mu\text{m}$, respectively. CP solutions were prepared by simply dissolving CP in methanol. However, CX/methanol solutions were prepared by dissolving CP in a 0.5 M MeONa/methanol solution.

is not affected by the rotational diffusion of the cyanophenol molecule in solution.³⁶ As mentioned in the Introduction, the positive peak corresponds to the 0–1 transition contributions such as ground-state bleach and stimulated emission, whereas the negative peak in the low-frequency region is for the 1–2 transition contribution originating from the excited-state absorption. Without detailed numerical analyses, the overall decaying patterns at first sight appear to be monotonic and exponential. However, a close inspection of the time-dependent changes of transient PP spectra reveals notable features and apparent deviation from an exponentially decaying function.

First of all, the 1–2 transition (negative) peak maximum shifts toward higher frequency. Second, the 0–1 transition (positive) peak is slightly blue-shifted as the waiting time T increases. If only one anharmonic oscillator is considered, such as the CN stretch mode in all CPs and CXs, the transient frequency shifting behaviors found in these T -dependent PP spectra cannot be easily explained. A directly related observation is that the long-time PP spectra appear to be notably different from those at a short time.

In Figure 5, we plot the normalized PP spectra, where the normalized spectrum at a given time T is defined as

$$\bar{S}(\omega, T) = \frac{S(\omega, T)}{\max[S(\omega, T)]} \quad (1)$$

Since these normalized spectra are corrected by removing the population relaxation contribution, the spectral line shape changes and peak frequency shifts are manifest in comparison to the original data shown in Figure 4. For the sake of clarity, we plot both the short- ($T = 100 \text{ fs}$) and long- ($T \approx 30 \text{ ps}$) time PP (normalized) spectra in Figure 6.

Regardless of the molecular structure and charge state, the normalized PP spectra in Figures 5 and 6 exhibit quite similar

spectral shifting patterns. For instance, let us examine the 2CX spectra (the top-right panel in Figure 5), that is, $\bar{S}(\omega, T)$ versus T . After a time T longer than a few picoseconds, the negative peak position shifts toward higher frequency by about 20 cm^{-1} , and simultaneously, the positive (0–1 transition) peak also undergoes a small blue shift. Even in the cases of CPs, such long-time PP spectral line shapes are fairly different from those at a short time. This suggests that there are at least two different vibrationally excited states, that their relative contributions to the PP spectrum change in time T , and that their lifetimes are different from each other. In the following section, we shall present detailed theoretical and numerical analysis results by considering a few different possibilities.

Discussion

Line Shape of a Frequency-Resolved Pump–Probe Spectrum. The transient frequency-resolved PP spectroscopy has been extensively used to study a number of ultrafast phenomena, and the corresponding theoretical descriptions have been presented before. From the theoretical work in ref 37, one can find that the transient PP spectrum can be approximated as a sum of two Gaussian functions, that is

$$S(\omega, T) \propto \left\{ 2 \exp\left(-\frac{(\omega - \omega_{10})^2}{2\Omega^2}\right) - C \exp\left(-\frac{(\omega - \omega_{21})^2}{2\Delta^2}\right) \right\} \exp(-T/\tau) \quad (2)$$

Here, the short-time approximation to the line-broadening function was used, and the vibrational spectral diffusion process was ignored because its frequency shift is usually very small.

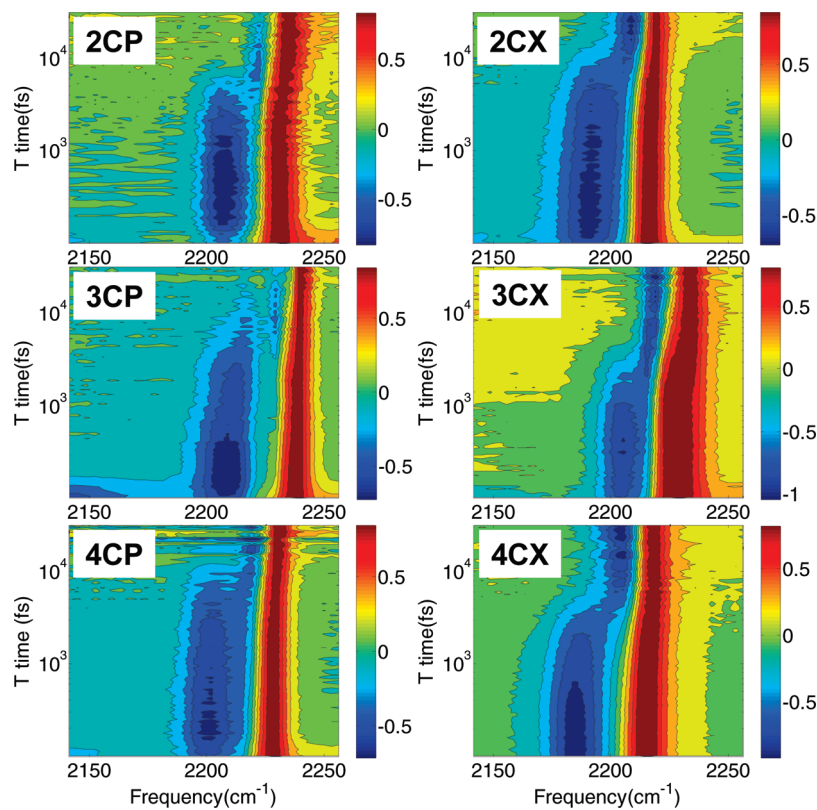


Figure 5. Normalized time-dependent frequency-resolved pump–probe spectra.

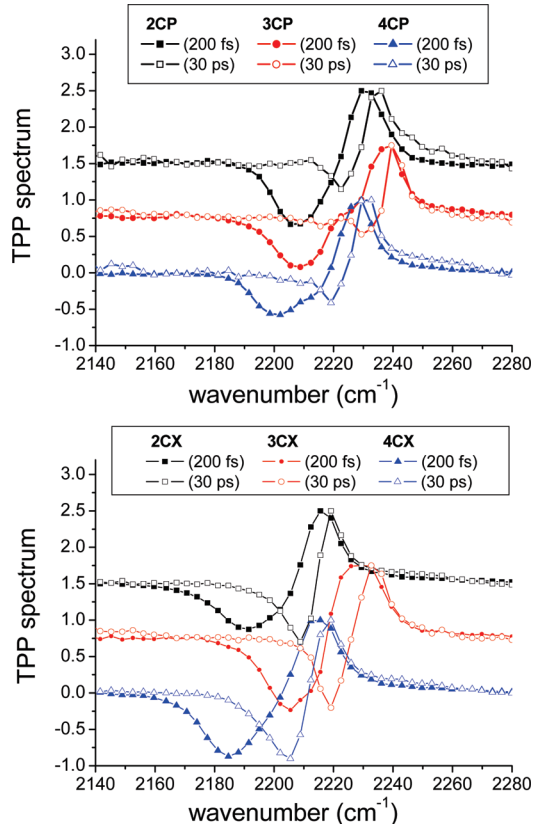


Figure 6. The short (200 fs) and long (30 ps) time (normalized) pump–probe spectra. Note that the PP spectrum shifts toward the higher-frequency region with time.

The first term in eq 2 originates from the sum of ground-state bleach and stimulated emission contributions that involve four optical transitions between the vibrationally ground and first

excited states. The second term in eq 2 represents the excited-state absorption. After the first two radiation–matter interactions with the pump field, the excited-state population is created. Then, the absorption of the probe field by the excited-state molecules occurs so that it contributes to the total PP signal as a negative contribution. Note that the line width of the 0–1 transition, denoted as Ω , can be different from that of the 1–2 transition, Δ , in general. Due to the overtone anharmonic frequency shift, $\delta\omega_{\text{anh}}$, we have

$$\omega_{21} = \omega_{10} - \delta\omega_{\text{anh}} \quad (3)$$

Within the harmonic approximation, since the 1–2 transition dipole moment is $2^{1/2}$ times larger than the 0–1 transition dipole moment, the relative weighting factor C of the excited-state absorption contribution is 2. However, in a real molecular vibration, due to the breakdown of the harmonic approximation to the potential energy curve, the weighting factor C is slightly different from 2, so that we shall consider it as a fitting parameter in this paper.

Lifetimes Measured with Integrated Photon Echo Experiments. Before we discuss detailed results from component analyses of experimentally measured PP spectra, the overall decay constants can be determined by using the time-resolved integrated photon echo signals. By using a single exponentially decaying function, the integrated photon echo signals of the CN stretch modes for all six molecular systems were fitted to $S_{\text{IPE}}(T) = S_{\text{IPE}}(T=0) \exp(-T/\tau_{\text{IPE}})$. The resultant decay constants are summarized in Table 1 (see the first row of this table).

The measured lifetimes of neutral cyanophenols are in the order 4CP > 2CP > 3CP. This is in fact in the same order for the resonance effects, which are manifest in the peak frequency of the CN stretch IR bands. On the other hand, in the cases of the anionic forms (2CX–4CX), the lifetime of 2CX is com-

TABLE 1: Exponential Decay Constants, τ_{IPE} , (in picoseconds) of the Time-Resolved Integrated Photon Echo Signals, Decay Constants of the Low- and High-Frequency Components, Denoted as τ_{LF} and τ_{HF} , 0–1 and 1–2 Transition Frequencies (cm^{-1}), Gaussian Line Widths (cm^{-1}), and Relative Weighting Factors C^a

	2CP	3CP	4CP	2CX	3CX	4CX
τ_{IPE} (ps)	1.9	1.3	3.1	3.1	1.2	1.6
τ_{LF} (ps)	1.8	1.0	2.8	3.1	1.2	1.4
τ_{HF} (ps)	2.1	2.1	4.1	4.8	1.5	1.6
$\omega_{\text{LF},10}$	2227	2232	2225	2212	2221	2209
$\omega_{\text{HF},10}$	2233	2240	2229	2219	2233	2217
$\omega_{\text{LF},21}$	2209	2206	2201	2190	2209	2183
$\omega_{\text{HF},21}$	2222	2223	2221	2209	2217	2205
Ω_{LF}	15.5	14.7	19.5	21.5	20.5	19.4
Ω_{HF}	8.8	20.5	15.1	15.8	7.1	19.4
Δ_{LF}	12.9	9.3	11.2	10.6	14.5	13.7
Δ_{HF}	17.3	7.4	8.7	8.8	12.9	11.1
C_{LF}	2.6	3.8	2.8	2.4	2.2	2.6
C_{HF}	1.2	1.6	2.0	2.6	1.4	2.4
N_{CN}	0.22	0.18	0.27	0.77	0.38	0.71
N_{OH}	0.73	0.74	0.73	2.66	3.1	2.8

^a The average numbers of H-bonded methanol molecules at the CN and the OH groups are denoted as N_{CN} and N_{OH} , respectively.

paratively longer than the other two, but that of 3CX is again the shortest one among the three cyanophenoxides. Although there is a subtle dependency of CN stretch lifetime on the molecular structure, the lifetimes show no strong correlations with the charge state of the molecule. This already indicates that the vibrational relaxation is determined by intramolecular processes, not by the solute–solvent interactions.

Frequency-Dependent Decay Constant. If there is only one anharmonic oscillator and the recovery time of the ground-state bleach is identical to the population relaxation time of the vibrational excited state, the overall amplitude of the PP spectrum should decrease exponentially. Consequently, the decay constant τ would not depend on frequency. In such a limiting case, the population relaxation measurement scheme by using the set of integrated photon echo signals or by carrying out a single exponential fitting to the transient PP data is enough to fully characterize the vibrational relaxation processes of cyanophenols. To test the validity of this single-species model, the time profile of the transient PP spectrum $S(\omega, T)$ at each frequency ω is fitted to a single exponential function as

$$S(\omega, T) = S(\omega, T = 0) \exp(-T/\tau(\omega)) \quad (4)$$

In Figure 7, the resultant decay constants $\tau(\omega)$ obtained are plotted.

One can immediately find that the decay constants are notably frequency-dependent. This suggests that more than one excited state (or band) is involved. In addition, we compared the decay constant of the 0–1 transition peak with that of the 1–2 transition peak (see the open circles in Figure 7). The 0–1 peak decays generally slower than the 1–2 peak does for all six cases, indicating that a low-frequency component has a longer lifetime in comparison to the high-frequency component, if there are two components (or two excited states) contributing to the PP signal.

Component Analysis with the Singular-Value Decomposition Method. In order to perform component analyses of time- and frequency-resolved PP spectra, which are functions of time and frequency, we used the singular-value decomposition (SVD)

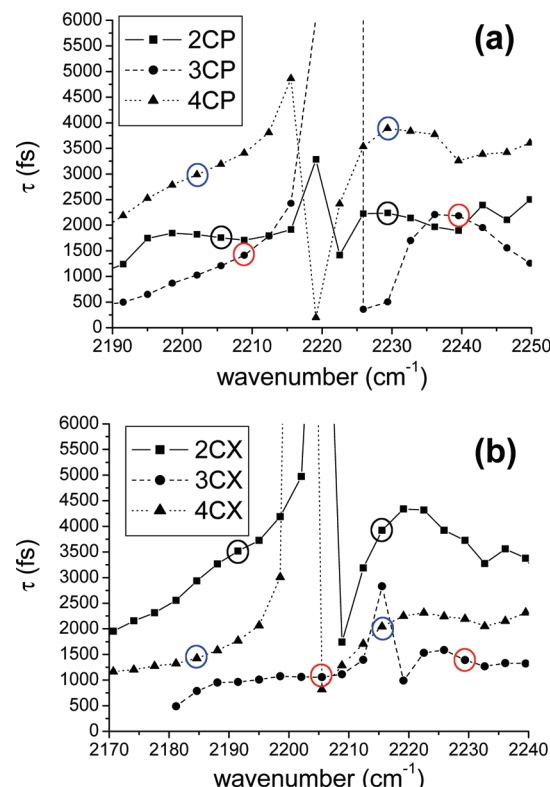


Figure 7. The frequency-dependent exponential decay constant. For a given frequency, the time profile of the transient PP signal is fitted with a single exponential function. Thus obtained decay constants are plotted with respect to the probe frequency. The open circles correspond to either the positive 0–1 peak or negative 1–2 peak. Usually, the negative 1–2 peak decays faster than the 0–1 peak.

method.^{38,39} The singular-value decomposition of the $S(\omega, T)$ matrix transforms it into a product of the time-dependent matrix $U(T)$, the singular-value matrix σ , and the frequency-dependent matrix $V(\omega)$ as

$$S(\omega, T) = U\sigma V^T \quad (5)$$

Here, σ is a diagonal matrix, and the magnitude of the diagonal matrix element, for example, $\sigma(j,j)$ represents the weight of the j th component. The eigenspectrum of the j th component is the j th column of the V matrix, and its time dependency corresponds to the j th column of the U matrix. For any given nonsquare matrix, the singular-value decomposition analysis can thus be performed to obtain the singular values and eigenspectra. However, the resultant eigenspectra do not necessarily represent the real spectra of involved chemical species. Thus, one should rely on an independent set of criteria to judge whether thus-obtained eigenspectra are reasonable and meaningful.

Bearing this aspect in mind, let us consider the transient PP spectra of 4CX. From the direct SVD analysis of $S(\omega, T)$, we found that the first two components account for 82%. The relative weights are 0.73 and 0.09. In Figure 8a and b, the corresponding eigenspectra and time profiles that are properly weighted by the corresponding singular values are plotted. The eigenspectrum of the major component, which will be denoted as $V_1(\omega)$, appears to be a typical PP spectrum exhibiting a negative–positive peak pattern (see eq 2). However, that of the minor component, $V_2(\omega)$, shows a negative–positive–negative peak pattern, and it cannot be considered as a pump–probe

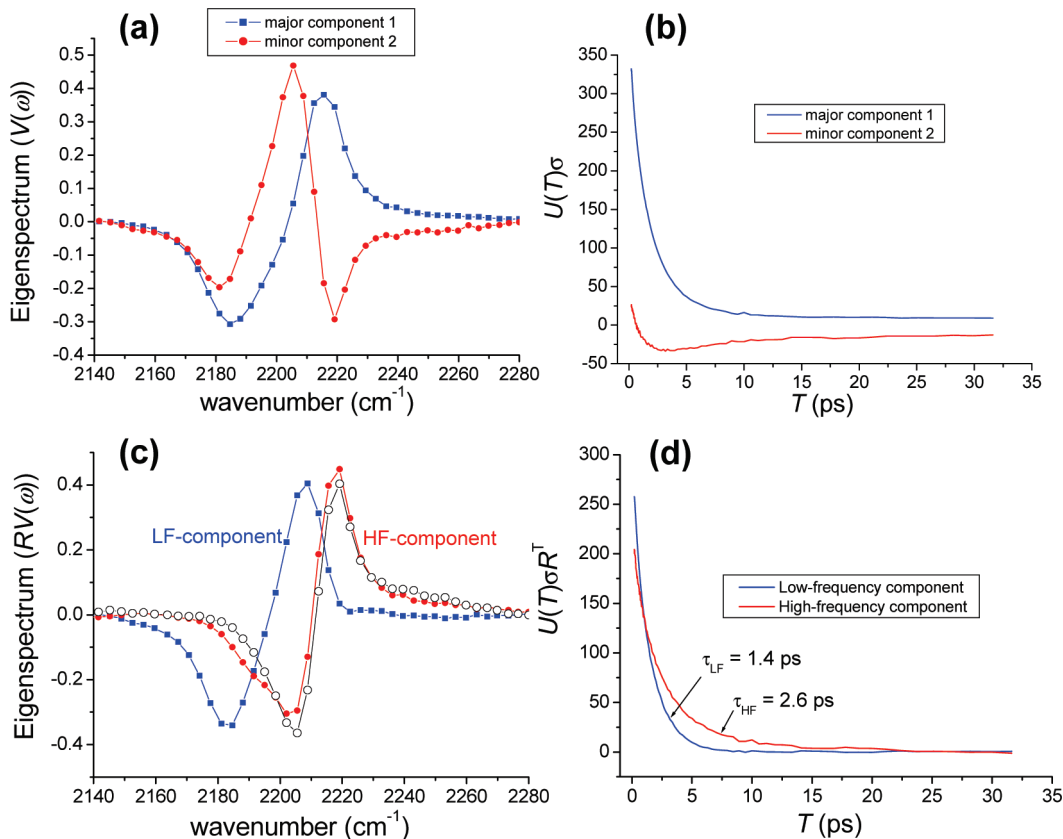


Figure 8. Singular-value decomposition analysis results of the transient PP spectral data $S(\omega, T)$ of 4CX. Considering the two major components, the eigenspectra of these two components are plotted in panel (a). Their time profiles are shown in panel (b). After applying a proper rotation procedure, the eigenspectra of the low- and high-frequency components are obtained (see panel (c)). The corresponding time profiles of the low- and high-frequency components are shown in panel (d). The exponential fitting constants are found to be 1.4 and 2.6 ps for the low- and high-frequency components, respectively.

spectrum of a single anharmonic oscillator. Furthermore, the time profile of the minor component decays to a negative value and then increases at a long time. This is again inconsistent with an intuitive picture.

To resolve these seemingly conflicting results, one can apply the rotation method to the SVD analysis. That is to say, by introducing a unitary matrix R that satisfies $R^T R = 1$, one can rewrite the singular-value decomposed matrix as

$$S(\omega, T) = U\sigma R^T R V^T \quad (6)$$

In the case of the two-species model, an obvious choice for the rotation matrix is

$$R = \begin{pmatrix} \cos \theta & -\sin \theta \\ \sin \theta & \cos \theta \end{pmatrix} \quad (7)$$

Considering θ as a parameter, one can obtain two new component spectra, $\tilde{V}_1(\omega, \theta)$ and $\tilde{V}_2(\omega, \theta)$, which are given as linear combinations of the original eigenspectra $V_1(\omega)$ and $V_2(\omega)$, as

$$\begin{aligned} \tilde{V}_1(\omega, \theta) &= V_1(\omega) \cos \theta - V_2(\omega) \sin \theta \\ \tilde{V}_2(\omega, \theta) &= V_1(\omega) \sin \theta + V_2(\omega) \cos \theta \end{aligned} \quad (8)$$

Then, the weighted time profiles are the column vectors of $U\sigma R^T$,

and they will be denoted as $F_1(T, \theta) = [U\sigma R^T]_1$ and $F_2(T, \theta) = [U\sigma R^T]_2$, where $[M]_j$ means the j th column of the matrix M .

Now, a set of criteria for determining the rotation angle θ is needed. First of all, the two transformed spectra $\tilde{V}_1(\omega, \theta)$ and $\tilde{V}_2(\omega, \theta)$ should have both negative and positive peaks that are characteristic features of PP spectrum. Second, the corresponding time profiles should behave normally and decay monotonically since there are no intermediate or product species in the present case. Third, the line shape of one of the two component spectra should be the same as the experimentally measured long-time PP spectrum since all six molecular systems show that their PP spectrum at a long time corresponds to that of the long-lived component among the two. Using these criteria, we determined the θ value, and it turns out to be $\pi/4$ in the case of 4CX, so that $\tilde{V}_1(\omega, \theta) = 2^{-1/2}\{V_1(\omega) - V_2(\omega)\}$ and $\tilde{V}_2(\omega, \theta) = 2^{-1/2}\{V_1(\omega) + V_2(\omega)\}$. These two transformed spectra are plotted in Figure 8c, and their line shapes are in accordance with a typical line shape of the PP spectrum. Second, the experimentally measured long-time PP spectrum (open circles in Figure 8c) of 4CX (shown in Figure 6 (the open triangles in the bottom panel) is directly compared with one of the two transformed spectra, $\tilde{V}_1(\omega, \theta)$ in this case; note that the overall amplitude of the experimentally measured long-time PP spectrum is properly scaled for the sake of comparison. The agreement is quantitative. Third, the time profiles, $F(T, \theta)$, of the low- and high-frequency components are also plotted in Figure 8d, and they are exponentially decaying with decay constants of 1.4 and 2.6 ps, respectively. Since the lifetime of the low-frequency component

is comparatively short, it disappears rapidly, and the long-time PP spectrum is thus dictated by the high-frequency component.

From the SVD analysis employing a proper rotation method, we clearly identified the two components whose spectra and time profiles are given in Figure 8c and d. In addition, the ratio of the initial value of the low-frequency component time profile to that of the high-frequency component, which was estimated to be about 1.6, gives the initial fractions or dipole strengths of the two components. The relative weights of the low-frequency components are larger than those of the high-frequency components, and they are in the range from 1.5 to 2.1.

By using the procedure outlined above, we carried out the SVD analyses for all of the other transient PP spectra, and the corresponding component spectra and decay constants were fully determined (see Supporting Information for detailed results for the other five cases, 2CP–3CX). The exponential decay constants of the low- and high-frequency components, denoted as τ_{LF} and τ_{HF} , respectively, are summarized in Table 1. In general, the low-frequency component, regardless of the relative position (ortho, meta, or para) of the substituent, has a shorter lifetime than the high-frequency component. This explains the experimental observation that the six PP spectra in Figure 4 show blue-shifting behaviors. The average lifetimes $\langle \tau \rangle = (\tau_{\text{LF}} + \tau_{\text{HF}})/2$ for the three neutral cyanophenols are in the same order as the resonance effect, that is, 4CP > 2CP > 3CP. However, in the cases of anionic forms, the lifetime of 2CX is the largest one among them, and the order is 2CX > 4CX > 3CX. Furthermore, the vibrational relaxation rate is comparatively fast when the substituent group is at the meta position. We shall return to this issue after the assignments of the two components are completed below.

Line Shape Analyses and Two Band Assignments. Now, from the eigenspectra and time profiles of the two components, the transient PP spectrum can be written as

$$S(\omega, T) = F_{\text{LF}}(T)\tilde{V}_{\text{LF}}(\omega) + F_{\text{HF}}(T)\tilde{V}_{\text{HF}}(\omega) \quad (9)$$

where the PP line shapes of the two components, for $j = \text{LF}$ and HF, can be approximately described as

$$\tilde{V}_j(\omega) \propto \left\{ 2 \exp\left(-\frac{(\omega - \omega_{j,10})^2}{2\Omega_j^2}\right) - C_j \exp\left(-\frac{(\omega - \omega_{j,21})^2}{2\Delta_j^2}\right) \right\} \quad (10)$$

Using this approximate expression for the dispersed PP spectra of the two components, we could determine the 0–1 and 1–2 transition frequencies ω_{10} and ω_{21} , line widths Ω and Δ , and relative transition strength C of the 1–2 transition contribution to the PP signal in comparison to that of 0–1 transition contribution. In Table 1, the fitting results are summarized.

Now, we shall address the question of what the two components are. First of all, one can easily rule out the possibility that the two components originate from dimer or aggregate formation since the UV-vis absorption and NMR spectra show no dependency on the solute concentration.

Second, from the values of 0–1 transition frequencies, $\omega_{\text{LF},10}$ and $\omega_{\text{HF},10}$, we found that the high-frequency modes are about 7 cm^{-1} blue-shifted from the low-frequency ones. From this observation, one might suggest that the two components are two solvation species differing from each other by the number of hydrogen-bonded solvent methanol molecules at the nitrile group. In refs 24 and 25, Hochstrasser and co-workers showed

that nitrile group in acetonitrile can form a single hydrogen bond with methanol. The CN stretch frequency of the single-hydrogen-bonded species is typically 8 cm^{-1} smaller than the one having no hydrogen bond. Recently, it was also shown that the nitrile can form two different types of H-bonds with protic solvent molecules. Depending on the H-bond angle (ϕ), the CN stretch mode frequency can be either blue- ($\phi > 120^\circ$) or red-shifted ($\phi < 120^\circ$). In solution, the H-bond angle has a distribution, and on average, the H-bond interaction of nitrile and protic solvent molecules has been found to induce a frequency blue shift.⁴⁰ This provided an explanation for why the CN group with a single H-bonded methanol molecule has an about 8 cm^{-1} larger frequency than that of the CN without a H-bond with methanol. Thus, at a low temperature, the FT-IR spectrum of the CN stretch of CH_3CN in methanol is a doublet; therefore, the chemical exchange 2D IR spectroscopy has been used to measure the H-bond-forming and -breaking rates. In our cases of the neutral and anionic cyanophenols, one might consider the two species, referred to as low- and high-frequency components here, to be these two different solvation species. However, this possibility can also be ruled out. From the fitting results in Table 1, one can calculate the overtone anharmonic frequency shifts, $\delta\omega_{\text{anh}} = \omega_{10} - \omega_{21}$. For the low-frequency components, we found that $\delta\omega_{\text{anh}}$ values are in the range from 18 to 26 cm^{-1} , except for the 3CX. On the other hand, $\delta\omega_{\text{anh}}$ values of the high-frequency components are much smaller than those of low-frequency components. If the high- and low-frequency components are associated with the CN stretch modes having one or zero hydrogen-bonded methanol molecule, it is expected that the overtone anharmonic frequency shifts of the two components should be almost the same as those found in the acetonitrile/methanol solution. Thus, we can ignore the possibility that the two components are related to the same CN stretch modes differing from each other by the solvation structure.

Third, we have examined the heating effects. In the pump–probe experiments, it has been well-known that the optical sample is heated by the repeated pump–field interactions. Fayer and co-workers studied the OD stretch of HOD in water and found that the transient PP spectrum at a sufficiently long time ($\sim 30 \text{ ps}$) corresponds to the difference absorption spectrum due to the temperature rise ($< 2^\circ\text{C}$).⁴¹ However, in our experimentally measured PP spectra for all six cases, we could not find any notably different PP spectral feature that is likely to be related to heating effects. For increasing temperature, we measured and examined the temperature-dependent IR absorption spectrum of CN stretch of 4CP in methanol and found no notable frequency shift induced by the temperature increases ($15 < T < 55^\circ\text{C}$), except for small line broadening. This indicates that the heating effect cannot be the source of frequency shifting behaviors found in our transient PP spectra.

After carefully examining the IR absorption and PP spectra, we finally concluded that there exists a combination state whose frequency is very close to the CN stretch frequency. An important clue can be found by studying the IR absorption spectrum of CH_3CN liquid. The CN stretch mode (ν_2) frequency is at 2253 cm^{-1} , but there is a strong combination band at 2293 cm^{-1} , which is the sum of the symmetric C–H bend (ν_3 : 1372 cm^{-1}) and the C–C stretch band (ν_4 : 918 cm^{-1}).⁴² The frequency difference between the CN stretch (ν_2) and the combination ($\nu_3 + \nu_4$) bands is about 40 cm^{-1} . However, in our cases of cyanophenols and their anions, the frequency differences between the CN stretches and the combination states are much smaller than the line widths of the two bands so that they merge

together and appear as a single peak in the IR spectra. Depending on the molecular structure and ionic state, the corresponding IR spectra appear to be slightly asymmetric or show a notable shoulder band. In order to examine the possibility of the existence of a combination band, we additionally measured IR spectra of benzonitrile in various aprotic solvents such as acetone, chloroform, and *n*-butanol. In all of these cases, we could identify a shoulder peak to the high-frequency region near the CN stretch peak (unpublished results). Furthermore, we measured the nonresonant Raman scattering spectra of these samples and found a notable shoulder band in the CN stretch peak too (see Figure S3 in Supporting Information). In addition, we carried out density function theory calculations (B3LYP/6-311**G++) of cyanophenols to obtain normal-mode frequencies and the corresponding eigenvectors. It is believed that the combination band is likely to be the combined benzene ring C=C stretch and C–H bend. However, it is extremely challenging and difficult to determine which combination mode is the one that is observed in the present experiments because calculations of the multidimensional potential energy surface of this molecule are not an easy task at all and are well beyond the scope of this work. Nevertheless, from all of these experimental observations discussed so far, we thus reach the conclusion that the low-frequency component is the CN stretch and the high-frequency component is a combination band.

This band assignment explains a number of experimental findings discussed in the present paper. The excited state of the combination mode has longer lifetime; therefore, its contribution to the PP spectrum is dominant at a long time. This is in turn the origin of the blue-shifting behaviors of the transient PP spectra (see Figure 4). Second, the fact that the anharmonic frequency shifts of high-frequency components are generally smaller than those of low-frequency components can be understood (see Table 1) because the high-frequency component is different from the CN stretch. Third, the existence of shoulders in the IR absorption spectra is due to these two vibrational transitions. Fourth, the relative ratios of the low-frequency component to the high-frequency component are more or less independent of the molecular structure and are in the range from 1.5 to 2.1. These values are related to the squares of dipole strengths of the CN stretch mode and the combination mode. Finally, the reason why the line widths Ω_{LF} and Δ_{LF} of the low-frequency component, which is the CN stretch, are notably different from those of the high-frequency component, which is the combination mode, can also be understood by the present assignment.

Before we close this subsection, we compare the present band assignment with the previous works on nitrile-derivatized compounds. In the Introduction, we mentioned that some nitrile-derivatized compounds and amino acids have been used as IR probes. For example, IR studies of cyanoalanine and thiocyanatoalanine were performed and showed that the CN stretch frequencies in these modified amino acids are highly sensitive to their local electric field and hydration environment. Unlike the cases of CPs and CXs, these nitrile-derivatized amino acids have no such combination modes whose frequencies are very close to that of the CN stretch mode. A more relevant work was reported by Hochstrasser and co-workers, who studied benzonitrile/methanol solution with a 2D IR measurement technique to determine the hydrogen-bond-making and -breaking rates. Unlike the case of benzonitrile, due to the substituted hydroxyl group in our cyanophenols, the normal and combination mode characters of CPs could be significantly different from those of benzonitrile. Yet, the other important IR probe that can be of use to study protein dynamics is the cyanlated

phenylalanine, which can also be easily incorporated into protein, as demonstrated by Getahun et al. in ref 19. This modified amino acid also contains a cyano group directly attached to the benzene moiety in the phenylalanine. Thus, it might be possible that an unknown combination band can also be in close proximity to the CN stretch band in this case. Consequently, it is necessary to carry out the same broad-band PP experiment for the cyanophenylalanine before any experimentally measured CN band frequency and line shape are used to study local electric field around its CN group.

Lifetimes of vibrationally excited States. Now, let us consider the relationship between the lifetime and the molecular structure again. The lifetime of the CN stretch mode of 3CP was found to be quantitatively similar to that of 3CX. This indicates that the lifetimes of the CN stretch modes in 3CP and 3CX are mainly determined by the intramolecular vibrational relaxation processes. Noting that the resonance effect in the 3CX is comparatively small, the lifetimes are not very dependent on the ionic state of the molecule. On the other hand, the lifetime of the CN stretch mode in 4CX is almost half of that of 4CP. Due to the resonance effect in 4CX, the population relaxation of the CN stretch is strongly influenced by the ionic state of the molecule. Interestingly, such a resonance effect makes the lifetime of the CN stretch mode in 2CX increase in comparison to that of 2CP. Unfortunately, further quantitative analyses and calculations of these subtle changes of population relaxation rates are beyond the scope of the present work; therefore, they are left for future studies.

QM/MM MD Simulations. To understand the vibrational dynamics of CN stretch modes in the six compounds that differ from one another by their electronic structures and their relations to the hydrogen-bonding interactions, we additionally carried out quantum mechanical/molecular mechanical molecular dynamics (QM/MM MD) simulation studies for all six solutions. Here, the solute molecule (CP or CX) was treated with a semiempirical QM method (PM3), and the solvent was classical. A detailed computational procedure for 4CP and 4CX only was discussed previously in ref 15.

In methanol solutions, both CP and CX can form strong hydrogen-bonding interactions with solvent molecules since both the nitrile and the hydroxyl (or phenoxide oxygen atom) groups are H-bonding sites. From the QM/MM MD trajectories, we first calculated the H-bond angle distribution (see Figure 9), where the H-bond angle is defined as $\angle \text{C}\equiv\text{N}\cdots\text{H}(\text{MeOH})$.

Regardless of the charge states of the CPs, the maximum distribution is at around 160°. Thus, this H-bond can induce a frequency blue shift of the CN stretch mode. Now, assuming that, if the distance between CN's nitrogen atom and methanol's H(OH) atom is less than 2.5 Å, it is considered a H-bond, and the average number, denoted as N_{CN} , of H-bonded methanol molecules around the CN group is calculated. The N_{CN} values of CXs are in general larger than those of CPs, as expected (see Table 1). This can also be understood by noting that the average atomic partial charges of the CN's nitrogen atom in CXs are typically twice larger than those in CPs (see Table 2). Nevertheless, they are less than 1.

We also calculated the average number, denoted as N_{OH} , of H-bonded methanol molecules at the OH group in CPs and at the phenoxide oxygen atom in CXs (Table 1). Again, the phenoxide oxygen atom that is highly negatively charged (see Table 2) usually forms more than two H-bonds with surrounding methanol molecules at a time. Although the number of H-bonded methanol molecules around the hydroxyl group in CPs does not depend on the relative (ortho, meta, or para) position of the OH group with

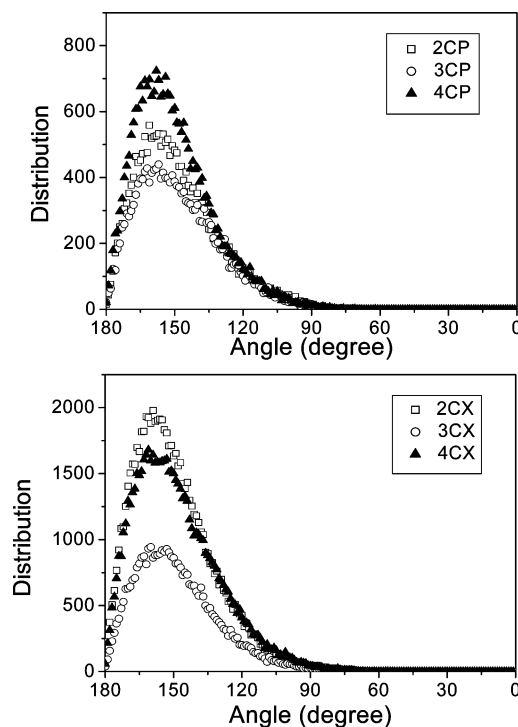


Figure 9. Distributions of hydrogen-bond angles ($\angle \text{C}=\text{N}\cdots\text{H}(\text{MeOH})$).

TABLE 2: Average Atomic Partial Charges (in electron's charge) of 2,3,4-Cyanophenols and 2,3,4-Cyanophenoxydes Obtained from PM3/MM MD Trajectories^a

atom type	atomic partial charges					
	2CP	3CP	4CP	2CX	3CX	4CX
N1	-0.126	-0.108	-0.128	-0.273	-0.177	-0.252
C1	-0.038	-0.062	-0.046	0.047	-0.030	0.023
C2	-0.055	0.045	-0.045	-0.271	0.066	-0.220
C3	-0.184	-0.137	-0.026	-0.300	-0.287	0.019
C4	-0.038	-0.146	-0.176	-0.017	-0.292	-0.328
C5	-0.147	-0.066	-0.177	-0.279	-0.039	-0.328
C6	-0.033	-0.109	-0.025	0.011	-0.245	0.019
H1	0.131	0.134	0.119	0.107	0.112	0.089
H2	0.112	0.128	0.131	0.086	0.107	0.109
H3	0.120	0.116	0.131	0.106	0.088	0.110
H4	0.119	0.123	0.119	0.088	0.109	0.089
C	0.144	0.102	0.132	0.380	0.326	0.362
OH(O)	-0.243	-0.248	-0.243	-0.684	-0.737	-0.691
HO	0.237	0.231	0.234			

^a N1 and C1 are the nitrogen and carbon atoms in the nitrile group, C is the carbon atom connected to the OH group, OH(O) is the oxygen atom in the CPs or CXs, and HO is the hydrogen atom of the OH group (see Supporting Information for the other atom types for these molecules).

respect to the CN group, that in CXs does strongly. Note that the meta-substituted cyanophenoxyde can form three H-bonds with methanol molecules on average. The order of N_{OH} is 3CX > 4CX > 2CX. In fact, this order is identical to that of the inverse lifetime, $1/\tau_{\text{LF}}$, of the CN stretch mode in CXs. This indicates that the excited-state energy of the CN stretch mode can be partially dissipated into the bath degrees of freedom through the interactions with methanol molecules that form strong H-bonds with the phenoxide oxygen atom in CXs.

From the QM/MM MD trajectories, we could also estimate the H-bond lifetimes for the series of CPs and CXs (Table 3). It turns out that the average lifetimes of the H-bonds between CN and methanol and those between CP's OH and methanol are about 10 ps. However, those between the phenoxide oxygen

TABLE 3: Average H-Bond Lifetime (ps) of 2,3,4-Cyanophenols and 2,3,4-Cyanophenoxydes Obtained from PM3/MM MD Trajectories^a

H-bond type	H-bond lifetime					
	2CP	3CP	4CP	2CX	3CX	4CX
CN $\cdots\text{HOMe}$	10.0	9.8	10.2	12.5	10.1	12.2
HO (O) $\cdots\text{H}(\text{MeOH})$	9.4	9.3	8.6	33.0	38.2	39.4
OH $\cdots\text{O}(\text{MeOH})$	11.8	11.3	11.1			

^a The H-bond type of parentheses indicates one of the cyanophenoxydes. The 10 fs time resolution is used for calculation of the H-bond lifetime, and the hydrogen bonding is treated within a distance of 3.0 Å between solute and solvent molecules.

atom in CX and methanol are significantly large, that is, ~ 35 ps. Experimentally, it was found that the existence, relative populations, and lifetimes of high- and low-frequency components do not strongly depend on the charge state of cyanophenol. Second, the frequency difference ($\sim 10 \text{ cm}^{-1}$) between the high- and low-frequency components is again independent of the latter. Consequently, it is possible to rule out the possibility that the low- and high-frequency components found in the analyses of transient PP spectra for all six compounds are related to the heterogeneous distributions of solvation species that differ from each other by the number of H-bonded methanol molecules at the OH or O⁻ sites. This is again consistent with the band assignments discussed in the previous subsection.

Summary and A Few Concluding Remarks

We carried out a variety of linear and nonlinear IR spectroscopy experiments to study vibrational dynamics of CN stretch modes in both neutral and anionic cyanophenols. Both ortho- and para-substituted cyanophenols are known to be stabilized by the resonance effect, whereas the meta-substituted cyanophenol does not. From the FT-IR studies of these six different cases, it was found that the vibrational frequency of the CN stretch mode is strongly red-shifted as the resonance effect increases. To study the acid–base reaction dynamics of 4-cyanophenol in methanol, we carried out chemical exchange 2D IR experiments. However, we could not find any notable cross peaks in the 2D IR spectra at times shorter than 5 ps. Note that the time-dependent cross peak amplitudes contain information on the rates of protonation and deprotonation reactions at the reactive site that is the hydroxyl group. This suggests that the acid–base reaction rates are slower than the lifetimes of the CN stretch mode. Currently, we are trying to improve the stability and experimental sensitivity of our 2D IR spectrometer and will carry out 2D IR measurements for a longer waiting time to find possible signatures of this acid–base reaction dynamics in solution.

To carefully examine the vibrational dynamics of CN stretch modes in these molecular systems, we carried out extensive transient PP experiments, where the pump–probe signal field was dispersed to obtain the frequency-resolved PP spectra for all six cyanophenols. It turns out that the lifetimes of neutral and anionic cyanophenols are dependent on precise molecular structures, that is, the para, meta, or ortho position of the OH group with respect to the CN group. However, the lifetimes of n CXs are not significantly different from those of n CPs. These observations suggest that the vibrationally excited state of the nitrile stretch mode in these cyanophenols predominantly relaxes to anharmonically coupled low-frequency intramolecular modes and not directly to the solvent degrees of freedom. Also, despite the fact that the hydrogen-bond strengths between the n CX anion and methanol molecules are much larger than those between

*n*CP and methanol, the intrinsic lifetimes do not change much. This clearly indicates that the hydrogen-bonding interaction between the OH (or O⁻) group and surrounding methanol molecules does not play a significant role in an early stage of vibrational energy relaxation processes.

In order to analyze the time-resolved PP spectra of multicomponent systems, we needed to develop a modified singular-value decomposition analysis method utilizing the rotation matrix. If there are multiple components with different lifetimes that contribute to the broad-band PP spectrum, one cannot use the conventional singular-value decomposition analysis because it does not provide physically meaningful results on the eigenspectra and populations of contributing components. We used this analysis method to fully characterize the time- and frequency-resolved PP spectra of cyanophenols and found that there is a combination band whose frequency is very close to the CN stretch frequency in these cases. Thus, even though the one-dimensional IR bands are spectrally congested and cannot be of use to separately study the CN stretch and combination mode, we were able to determine the anharmonic frequency shifts, lifetimes, line widths, and relative dipole strengths of both the CN stretch and combination modes by analyzing the time-resolved PP spectra and employing a properly modified SVD analysis method. This is quite important because the component analysis of a given IR absorption spectrum based on least-squares fitting to experimental data with multiple Gaussian, Lorentzian, or combination of these two functions can be arbitrary and erroneous. However, if the two components have different lifetimes, the time-resolved PP spectroscopy can separate these two spectra, as has been demonstrated in this paper. Thus, there is no ambiguity in assigning the two components.

Overall, we have shown that the linear and nonlinear IR spectroscopic methods can provide a detailed picture of the resonance effects on the vibrational frequency and energy relaxation and be of use to study vibrational dynamics of multicomponent systems. In order to carefully examine the nature of the combination mode found in the present work, we shall carry out isotopic replacement experiments. For instance, deuterated cyanophenols can be interesting molecular systems because the frequency shifts of the C—D bending modes in comparison to the benzene C—H bending mode frequencies could induce significant changes of the frequencies of the combination modes found in this work. This will result in a spectrally separated CN stretch band from any possible combination bands. Also, currently, we are trying to carry out 2D IR chemical exchange experiments to study possible dimer formation—dissociation dynamics of certain cyanophenols in an aprotic solvent. It is noted that the nitrile of a given CP can form a hydrogen bond with the hydroxyl group of a neighboring CP molecule when they are dissolved in an aprotic solvent. This can be viewed as a simple prototype model system for a Watson—Crick base pair formation. Thus, studying such a cyclic dimer formation process in the condensed phase will provide us with information on the time scale and mechanism of the hydrogen-bonding dynamics.

Acknowledgment. This work was supported by the grant (No. 20090078897) of NRF/MEST to M.C.

Supporting Information Available: Concentration-dependent UV-vis absorption and IR spectra of 4-cyanophenol in methanol, Raman scattering spectra of *n*CPs in methanol, singular-value decomposition analysis results, and definitions of atom types of *n*CPs and *n*CXs. This material is available free of charge via the Internet at <http://pubs.acs.org.org>.

References and Notes

- (1) Marder, S. R.; Beratan, D. N.; Cheng, L. T. *Science* **1991**, 252, 103–106.
- (2) Gorman, C. B.; Marder, S. R. *Proc. Natl. Acad. Sci. U.S.A.* **1993**, 90, 11297–11301.
- (3) Marder, S. R.; Gorman, C. B.; Tiemann, B. G.; Cheng, L. T. *J. Am. Chem. Soc.* **1993**, 115, 3006–3007.
- (4) Andraud, C.; Brotin, T.; Garcia, C.; Pelle, F.; Goldner, P.; Bigot, B.; Collet, A. *J. Am. Chem. Soc.* **1994**, 116, 2094–2102.
- (5) Bourhill, G.; Bredas, J. L.; Cheng, L. T.; Marder, S. R.; Meyers, F.; Perry, J. W.; Tiemann, B. G. *J. Am. Chem. Soc.* **1994**, 116, 2619–2620.
- (6) Marder, S. R.; Cheng, L. T.; Tiemann, B. G.; Friedli, A. C.; Blancharddesce, M.; Perry, J. W.; Skindhoj, J. *Science* **1994**, 263, 511–514.
- (7) Albert, I. D. L.; Marks, T. J.; Ratner, M. A. *J. Phys. Chem.* **1996**, 100, 9714–9725.
- (8) Reinhardt, B. A.; Brott, L. L.; Clarson, S. J.; Dillard, A. G.; Bhatt, J. C.; Kannan, R.; Yuan, L. X.; He, G. S.; Prasad, P. N. *Chem. Mater.* **1998**, 10, 1863–1874.
- (9) Belfield, K. D.; Schafer, K. J.; Mourad, W.; Reinhardt, B. A. *J. Org. Chem.* **2000**, 65, 4475–4481.
- (10) Cho, B. R.; Son, K. H.; Lee, S. H.; Song, Y. S.; Lee, Y. K.; Jeon, S. J.; Choi, J. H.; Lee, H.; Cho, M. *J. Am. Chem. Soc.* **2001**, 123, 10039–10045.
- (11) McKelvey, J. M.; Alexandratos, S.; Streitwieser, A.; Abboud, J. L. M.; Hehre, W. J. *J. Am. Chem. Soc.* **1976**, 98, 244–246.
- (12) Hehre, W. J.; Pople, J. A.; Random, L. *J. Am. Chem. Soc.* **1972**, 94, 1496.
- (13) Stock, L. M.; Brown, H. C. *Adv. Phys. Org. Chem.* **1963**, 1, 35–154.
- (14) Hoggett, J. G.; Moodie, R. B.; Penton, J. R.; Schofield, K. *Nitration and Aromatic Reactivity*; Cambridge University Press: Cambridge, U.K., 1971.
- (15) Ha, J.-H.; Lee, K.-K.; Park, K.-H.; Choi, J.-H.; Jeon, S.-J.; Cho, M. *J. Chem. Phys.* **2009**, 130, 9.
- (16) Georgieva, M. K.; Angelova, P. N.; Binev, I. G. *J. Mol. Struct.* **2004**, 692, 23–35.
- (17) Oh, K.-I.; Lee, J.-H.; Joo, C.; Han, H.; Cho, M. *J. Phys. Chem. B* **2008**, 112, 10352–10357.
- (18) Helbing, J.; Bonacina, L.; Pietri, R.; Bredenbeck, J.; Hamm, P.; van Mourik, F.; Chaussard, F.; Gonzalez-Gonzalez, A.; Chergui, M.; Ramos-Alvarez, C.; Ruiz, C.; Lopez-Garriga, J. *Biophys. J.* **2004**, 87, 1881–1891.
- (19) Getahun, Z.; Huang, C. Y.; Wang, T.; De Leon, B.; DeGrado, W. F.; Gai, F. *J. Am. Chem. Soc.* **2003**, 125, 405–411.
- (20) Fang, C.; Bauman, J. D.; Das, K.; Remorino, A.; Arnold, E.; Hochstrasser, R. M. *Proc. Natl. Acad. Sci. U.S.A.* **2008**, 105, 1472–1477.
- (21) Choi, J.-H.; Oh, K.-I.; Cho, M. *J. Chem. Phys.* **2008**, 129, 174512.
- (22) Fang, C.; Bauman, J. D.; Das, K.; Remorino, A.; Arnold, E.; Hochstrasser, R. M. *Proc. Natl. Acad. Sci. U.S.A.* **2008**, 105, 1472.
- (23) Krummel, A. T.; Zanni, M. T. *J. Phys. Chem. B* **2008**, 112, 1336–1338.
- (24) Kim, Y. S.; Hochstrasser, R. M. *Proc. Natl. Acad. Sci. U.S.A.* **2005**, 102, 11185–11190.
- (25) Kim, Y. S.; Hochstrasser, R. M. *J. Phys. Chem. B* **2006**, 110, 8531–8534.
- (26) Ghosh, A.; Remorino, A.; Tucker, M. J.; Hochstrasser, R. M. *Chem. Phys. Lett.* **2009**, 469, 325–330.
- (27) Cho, M. *Two-Dimensional Optical Spectroscopy*; CRC Press: Boca Raton, FL, 2009.
- (28) Nibbering, E. T. J.; Elsaesser, T. *Chem. Rev.* **2004**, 104, 1887–1914.
- (29) Tokmakoff, A. *J. Phys. Chem. A* **2000**, 104, 4247–4255.
- (30) Woutersen, S.; Mu, Y.; Stock, G.; Hamm, P. *Chem. Phys.* **2001**, 266, 137–147.
- (31) Kim, Y. S.; Hochstrasser, R. M. *Proc. Natl. Acad. Sci. U.S.A.* **2005**, 102, 11185–11190.
- (32) Kwac, K.; Lee, H.; Cho, M. *J. Chem. Phys.* **2004**, 120, 1477.
- (33) Zheng, J.; Kwac, K.; Asbury, J. B.; Chen, X.; Piletic, I.; Fayer, M. D. *Science* **2005**, 309, 1338–1343.
- (34) Zheng, J.; Kwac, K.; Fayer, M. D. *Acc. Chem. Res.* **2007**, 40, 75–83.
- (35) Cho, M. *Chem. Rev.* **2008**, 108, 1331–1418.
- (36) Tan, H. S.; Piletic, I. R.; Fayer, M. D. *J. Opt. Soc. Am. B* **2005**, 22, 2009–2017.
- (37) Kwac, K.; Cho, M. *J. Phys. Chem. A* **2003**, 107, 5903.
- (38) Henry, E. R.; Hofrichter, J. *Methods Enzymol.* **1992**, 210, 129–192.
- (39) Goldbeck, R. A.; Kliger, D. S. *Metallobiochemistry, Part C*; Academic Press Inc: San Diego, CA, 1993; Vol. 226, pp 147–177.
- (40) Choi, J.-H.; Oh, K.-I.; Lee, H.; Lee, C.; Cho, M. *J. Chem. Phys.* **2008**, 128, 134506.
- (41) Steinel, T.; Asbury, J. B.; Zheng, J. R.; Fayer, M. D. *J. Phys. Chem. A* **2004**, 108, 10957–10964.
- (42) Zhao, W.; Wright, J. C. *J. Am. Chem. Soc.* **1999**, 121, 10994–10998.